Short Lectures - C, Tuesday, June 12

SL - C1

NEUTRON DIFFRACTION EXAMINATION OF THE TEXTURES OF ZIRCONIUM BASED ALLOYS

M. Kučeráková[1], S. Vratislav[1], Z. Trojanová[2]

[1]Department of Solid State Engineering, FNSPE, CTU, Trojanova 13, 120 00, Prague 2, Czech Republic
[2]Faculty of Mathematics and Physics, Ke Karlovu 5, 121 16, Czech Republic
monika.kucerakova@fjfi.cvut.cz

Introduction

Neutron diffraction texture analysis is used extensively in research into the preferential orientation of zirconium based alloys used in nuclear technique [1]. Textures of five zirconium samples labeled as ZZ were investigated by using inversion pole figures. The texture measurements were performed on the KSN-2 neutron diffractometer located at the research reactor LVR-15 in the Nuclear Research Institute, plc. Rez, Czech Republic. Collected data were processed by software package GSAS. The wavelength used was = 0.1362 nm.

Samples

We had series of five zirconium samples labeled as ZZ. Fig. 1 shows shape and dimensions of samples. Four samples (ZZ14, ZZ19, ZZ16 and ZZ17) were deformed by uniaxial tension by using mechanical testing system ISNTRON 5882. Tab. 1 shows parameters of the experiment. Structure of the initial (non-deformed by uniaxial tension) sample ZZ13 observed by using light microscope Zeiss Axio Imager ZM1 is in Fig. 2.

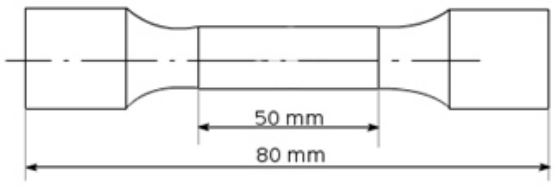

Figure 1. Shape and dimensions of ZZ samples

Figure 2. Structure of initial sample ZZ13 observed by light microscope Zeiss Axio Imager ZM1.

Table 1. Parameters of uniaxial tension experiment.

Sample	[%]	[MPa]
ZZ14	6	121
ZZ19	10	124
ZZ16	15	134
ZZ17	20	146

Inverse pole figures

The intensity ratios p_{hkl},q were calculated by Mueller formula for (100), (002), (101), (102), (110), (103), (112) and (201) reflections for directions q = TD, ND, RD, see Tab. 2.

Table 2. Calculated inverse pole figures of ZZ samples.

Sample	**13**	**14**	**9**	**16**	**17**
$\mathbf{p_{002,\ TD}}$	1.3	1.9	1.8	2.1	2.3
$\mathbf{p_{002,\ ND}}$	2.8	2.7	2.6	2.8	3.1
$\mathbf{p_{002,\ RD}}$	0.1	0.1	0.1	0	0
$\mathbf{p_{100,\ TD}}$	1.0	0.7	0.5	0.6	0.5
$\mathbf{p_{100,\ ND}}$	0.4	0.5	0.4	0.5	0.4
$\mathbf{p_{100,\ RD}}$	2.6	3.2	4.3	3.8	4.0
$\mathbf{p_{110,\ TD}}$	0.8	0.8	0.7	0.7	0.9

Discussion and Conclusions

Our results can be summarized as follows:

- Samples prefer orientation of planes (100) and (110) perpendicular to rolling direction.
- Basal planes are oriented perpendicular to normal direction.
- The texture increases with deformation.

Zirconium based alloys are used in nuclear technology, and our results are consistent with data published by the other authors [3].

Acknowledgments

This research has been supported by the Ministry of Industry and Trade of the Czech Republic grant MPOFRTI1 -378.

References

1. H. Hsun, *Texture of metals*, Technical report, United States Steel Corporation Research Laboratory, 1974.
2. G. E. Bacon, *Neutron Diffraction*, 3rd ed., Oxford: Clarendon Press, 1975.
3. A. V. Nikulina, *Zirconium Alloys in Nuclear Power Engineering*, Metal Science and Heat Treatment, 46, 2004, pp. 458 – 462.

SL - C2

PHASE TRANSFORMATIONS OF E110G Zr-ALLOY OBSERVED BY "IN-SITU" XRD

J. Říha, P. Šutta

University of West Bohemia, New Technologies - Research Centre, Univerzitní 8, 306 14 Plzeň
Czech Republic
janriha@ntc.zcu.cz

The most important area of zirconium alloys usage is today the nuclear energetics. In this sphere the zirconium alloys are mainly used as protective layers of nuclear fuel rods where they create a first barrier against the reactor core atmosphere. For this application the Zr-alloys must ensure a very low absorption cross section for thermal neutrons, high corrosion resistance in water steam at high pressure and temperature a good mechanical properties. In this form these alloys are used in pressurized- and boiling-water reactors. Except of those properties zirconium has a strong affinity for gaseous oxygen, nitrogen and hydrogen with which they can form stable oxides, nitrides and hydrides [1, 2]. Physical and mechanical properties of zirconium are influenced especially by oxygen presence significantly. In form of solid solution oxygen and also nitrogen stabilize the low-temperature -Zr modification with HCP lattice and also increase the zirconium hardness. The phase transformation temperature of pure zirconium is 863 °C, Fig. 1 and 2.

The development of new Zr-alloys is in nowadays focused on their behaviour optimisation during the Loss of Coolant Accident (LOCA). This type of reactor accident results in a rapid moderator escape in time shorter than 10 seconds, followed by a rapid heating of the Zr-alloy in steam environment at the temperature above 1000°C. These severe conditions lead partly to a fast high-temperature oxidation and also to a phase transformation of Zr-alloy to high-temperature -modification with body-centred cubic lattice structure until the reactor core is flood with water and the cladding is quenched back to -phase. The temperature of Zr-alloy phase transformation is strongly influenced by free oxygen and nitrogen placed in interstitial positions of crystal lattice and also by a heating rate [3], Fig. 1 and 2.

The Zr-Nb alloy E110G was used as an experimental material, Tab. 1. This material is today most often used for nuclear fuel rods protective layers. With regard to interstitial oxygen and nitrogen influence on phase transformations the samples of pure Zr supplied by Goodfellow Ltd. were used for the comparison. During previous experiments [4, 5] was observed, that the phase transformation of zirconium to -phase did not proceed even at 1000°C. On the basis of that, the experimental samples were heated at three temperatures, 1100 °C, 1150 °C and 1200 °C. After that, the samples were cooled down at 1000 °C, 900 °C 800 °C and 30 °C, Fig 3. The diffraction patters were recorded at all these temperatures.

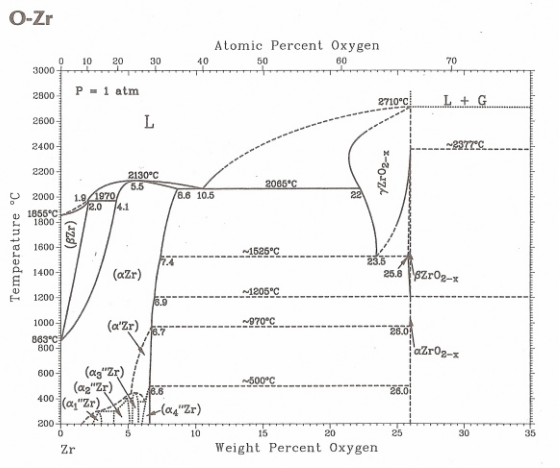

Figure 1. Zirconium – oxygen binary phase diagram.

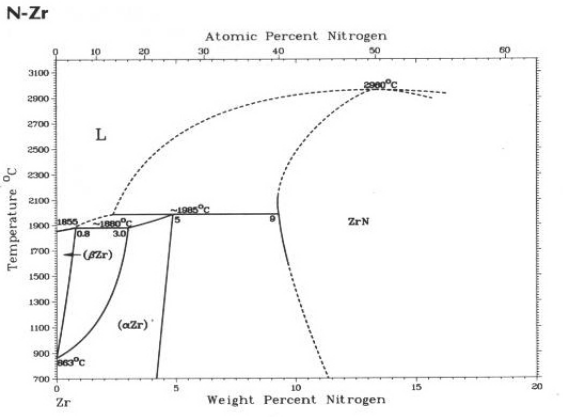

Figure 2. Zirconium – nitrogen binary phase diagram.

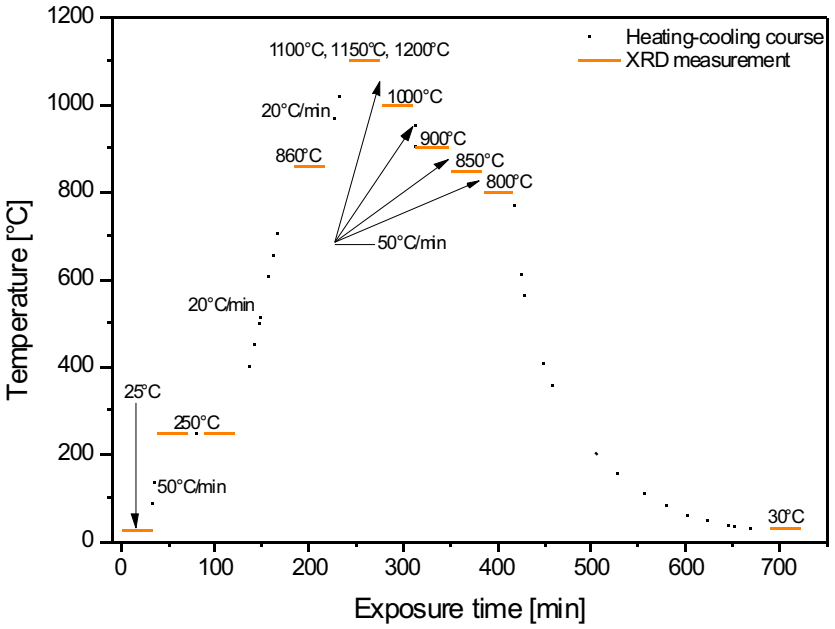

Figure 3. Heat treatment of experimental samples.

Table 1. Chemical composition of E110G Zr-Nb alloy.

E110G Alloy	Element							
	Nb [%]	Fe [ppm/%]	H [ppm]	N [ppm]	C [ppm]	O [ppm]	Ni [ppm]	Hf [ppm]
	1,0 - 1,1	0,055	3	20	100	840	-	~500

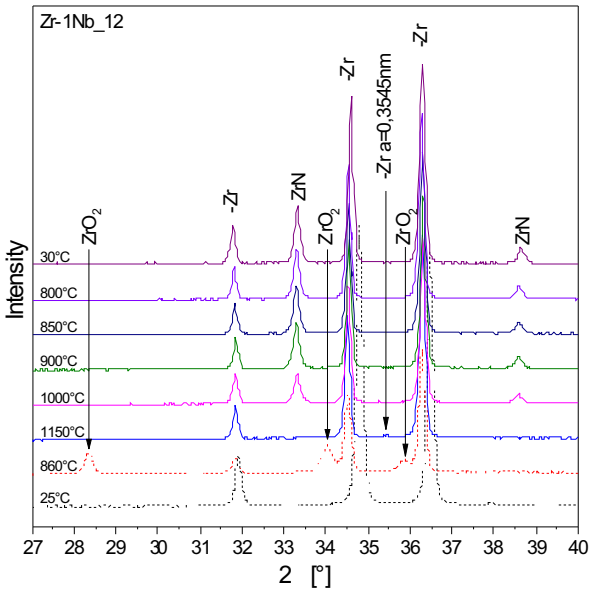

Figure 4. Partial diffraction pattern of Zr-1Nb_12.

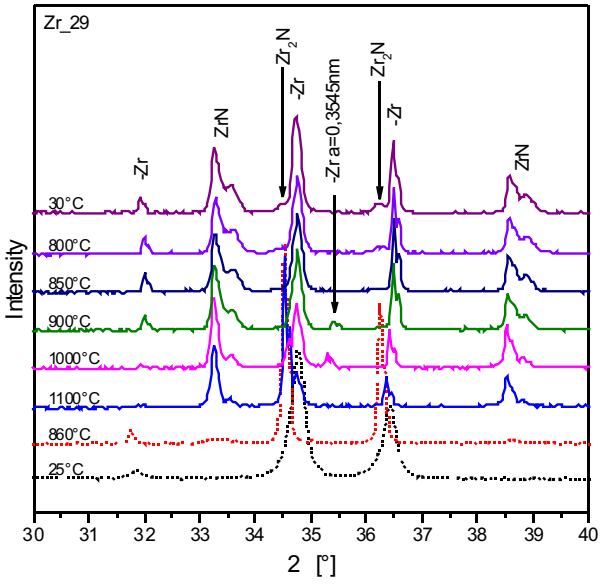

Figure 5. Partial diffraction patterns of Zr_29.

The XRD measurements proceeded in high-temperature chamber Anton Paar HTK 1200N being a part of automatic powder diffractometer Panalytical X'Pert Pro. This instrument uses a copper X-ray tube ($_K$ = 0.15406 nm) and an ultra-fast semiconductor detector PIXcel. The chamber was evacuated with the aid of turbo-molecular pump Edwards EXT75DX. A dry scroll pump Edwards XDS5 created the initial vacuum. For the lowest pressure achieving, the deaeration step at 250 °C for 60 minutes was applied on the samples.

From the XRD results of both types of experimental materials is evident that they contain a significant amount of nitrogen. This element is in all samples in form of solid solution – diffraction patterns of both samples in initial state show only a presence of -Zr phase. The nitrogen

causes an expressive increasing of phase transformation temperature, Fig. 2.

A trace amount of high-temperature -Zr phase can be identified in E110G alloy after heating at 1150 °C, sample Zr-1Nb_12, Fig. 3. This is mainly caused by interstitial nitrogen but also by interstitial oxygen which is contained in the material structure already in initial state, Tab. 1. That is why the -Zr phase is unstable under 1000 °C and transforms back to low temperature -Zr. Due to high amount of interstitial nitrogen in the structure also a zirconium nitride ZrN have created on the sample surface during the cooling from 1150 °C to 1000 °C. In the case of pure zirconium, sample Zr_29, the small amount -Zr phase created already after the heating at 1100°C, but during the cooling down at 1000 °C. This is caused by -Zr surface layer depletion of nitrogen which is used for creation of surface ZrN layer, Fig. 4. During the subsequent cooling down, the residual interstitial nitrogen amount in the structure of zirconium decreases and the phase transformation of -Zr to low-temperature -phase proceeds in accord with the binary phase diagram Zr - N, Fig. 5.

1. M. E. Dric,: Svojstva elementov, spravočnik, Metallurgija Moskva 1985

2. J. Koutský, J. Kočík,: Radiation damage of structural materials. Praha Academia, 1994.

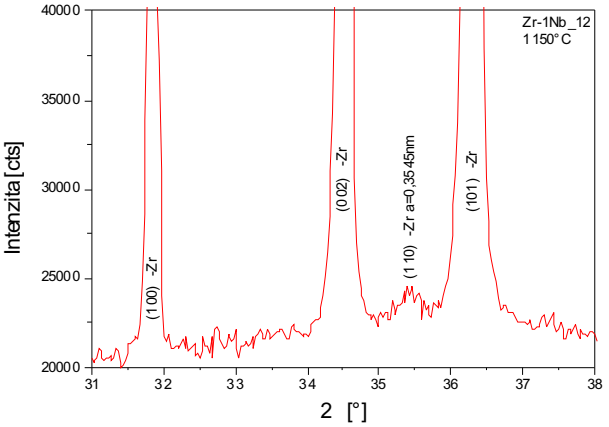

Figure 5. Partial diffraction pattern of Zr_29 during the heating.

3. A. R. Massih, *J. Nucl. Mat.*, **384**, (2009), pp. 330–335

4. J. Říha, O. Bláhová, P. Šutta, *Chemické listy*, **105**, (2011), pp. 210-213.

5. J. Říha, R. Medlín, A. Vincze, P. Šutta, *Vacuum*, **86**, (2012), pp. 785-788.

SL - C3

SHAPE MEMORY ALLOY Co-Ni-Al AS COMPLEX MULTIFERROIC

J. Kopeček[1], M. Jarošová[2], K. Jurek[2], J. Drahokoupil[1], I. Kratochvílová[1], L. Fekete[1], L. Bodnárová[3], H. Seiner[3], P. Sedlák[3], M. Landa[3], J. Šepitka[4], J. Lukeš[4], V. Kopecký[1], O. Heczko[1]

[1]Institute of Physics of the AS CR, Na Slovance 2, 182 21 Praha 8, Czech Republic
[2]Institute of Physics of the AS CR, Cukrovarnická 10/112, 162 00 Praha 6, Czech Republic
[3]Institute of Thermomechanics of AS CR, Dolejškova 5, 182 00 Prague 8, Czech Republic
[4]Laboratory of Biomechanics, CTU in Prague, Technická 4, 166 07, Prague 6, Czech Republic
kopecek@fzu.cz

Great success in Ni_2MnGa derived alloys [1,2] attracted attention towards similar Heusler alloys including cobalt based CoNiAl and CoNiGa [3,4]. As the NiMnGa alloys suffer due to their strongly intermetallic state (brittleness, poor creep and fatigue properties) the cobalt based alloys seemed to be the interesting candidate for the mechanically stronger and more resistant FSMAs.

The article describes the progress in work on $Co_{38}Ni_{33}Al_{29}$ alloy [5,6]. The defined crystals with single-crystalline matrix were prepared after long struggling. The influence of annealing on martensitic transformation was investigated. Both post-mortem XRD and in-situ neuron diffraction confirmed the martensitic phase transformation of alloy matrix B2 $L1_0$ and stable amount of A1 particles (fcc cobalt solid solution) in alloy, Fig. 1. The image of transformation paths is blurred considering the results of resonant ultrasound spectroscopy (RUS), magnetic susceptibility measurements and various microscopies (LOM, SEM, AFM), which shows transformation temperature significantly higher (about approx. 70 °C). The strong premartensitic phenomena can be documented by the evolution of damping in RUS. Regardless to structural confusion all samples exhibit pseudoelastic behaviour at room temperature, which is strongly dependent on crystallographic orientation as shown in Fig. 2.

Authors would like to acknowledge the financial support from the Grant Agency of the AS CR project IAA1001009 20 and Czech Science Foundation projects 101/09/0702, P107/11/0391 and P107/10/0824.

1. Heczko O., Scheerbaum N., Gutfleisch O., *Magnetic Shape Memory Phenomena*, in *Nanoscale Magnetic Materials and Applications*, edited by J.P. Liu et al. (Springer Science+Business Media, LLC), 2009, pp. 14-1.

2. Heczko O, Sozinov A, Ullakko K, *IEEE Trans. Magn.*, **36**, (2000), 3266-3268.

3. K. Oikawa, L. Wulff, T. Iijima, F. Gejima, T. Ohmori, A. Fujita, K. Fukamichi, R. Kainuma, K. Ishida, *Appl. Phys. Lett.*, **79**, (2001), 3290.

4. Yu. I. Chumlyakov, I. V. Kireeva, E. Yu. Panchenko, E. E. Timofeeva, Z. V. Pobedennaya, S. V. Chusov, I. Karaman, H. Maier, E. Cesari and V. A. Kirillov, *Russ. Phys. J.,* **51**, (2008), 1016.

5. J. Kopeček, S. Sedláková-Ignácová, K. Jurek, M. Jarošová, J. Drahokoupil, P. Šittner, V. Novák: *Structure development in $Co_{38}Ni_{33}Al_{29}$ ferromagnetic shape memory alloy*, 8th th European Symposium on Martensitic Transformations, ESOMAT 2009, edited by Petr Šittner, Václav Paidar, Luděk Heller, Hanuš Seiner, 2009, article No. 02013.

6. J. Kopeček, K. Jurek, M. Jarošová, et al., *IOP Conf. Sci.: Mater. Sci. Eng.*, **7**, (2010), 012013.

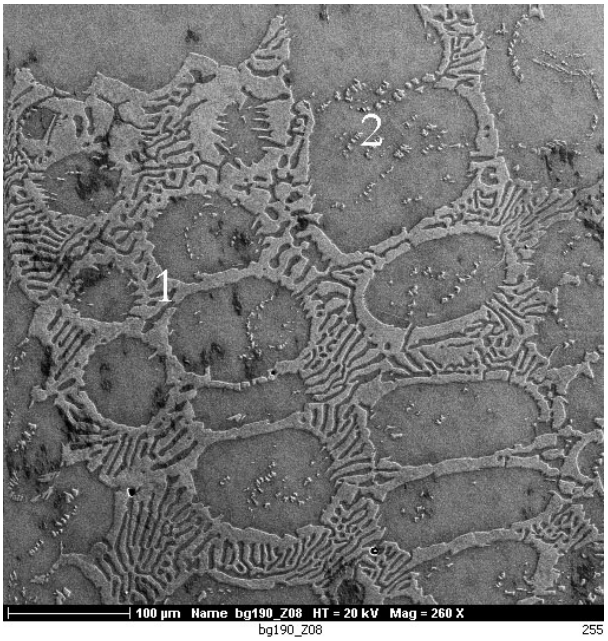

Figure 1. The structure of the samples observed by scanning electron microscopy. The precipitates marked 1 are interdendritic A1 fcc cobalt solid solution particles. The precipitates marked 2 are $L1_2$ ordered precipitates of the phase $(Co,Ni)_3Al$.

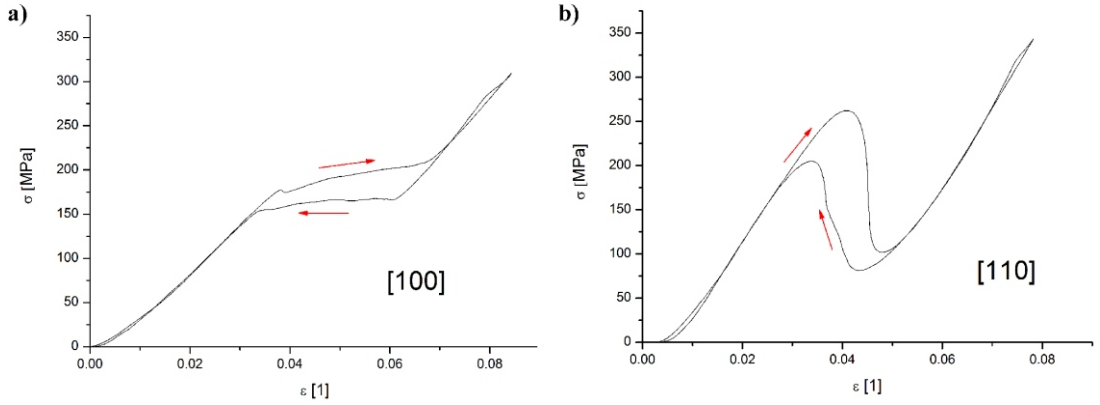

Figure 2. Superelastic behaviour in $Co_{38}Ni_{33}Al_{29}$ alloy single-crystals is strongly dependent on orientation. The measurement were performed at room temperature with deformation rate 0,1 s^{-1}.

SL - C4

DIFFRACTION STUDY OF RESIDUAL STRESS DEPTH DISTRIBUTION IN SURFACE LAYERS OF SHOT-BLASTED DECARBURISED STEELS

K. Kolařík, N. Ganev, Z. Pala, J. Drahokoupil

Department of Solid State Engineering, Faculty of Nuclear Sciences and Physical Engineering, Czech Technical University in Prague, Trojanova 13, 120 00 Prague
kamil.kolarik@email.cz

Surface decarburization of construction steels occurs during their forging, drawing and casting. As a softening process, decarburization leads to a considerable fatigue limit decrease. This detrimental effect can be reduced by strengthening the decarburised layer using plastic deformation induced by shot peening. As a result compressive residual stresses are created in the surface layer.

The aim of the contribution is to present the results of X-ray diffraction analysis of residual stress depth profiles in surface layers of sand-blasted and shot-blasted steels. Depth distributions of macroscopic (first-order) residual stresses were determined up to approx. 500 µm beneath the blasted surface.

extended abstract submitted